第32卷第3期 红外与毫米波学报 Vol. 32, No. 3
2013年6月 J. Infrared Millim. Waves June, 2013

文章编号:1001-9014(2013)03-0193-06 DOI:10.3724/SP.J.1010.2013.00193

High performance InP-based $In_{0.52}Al_{0.48}As/In_{0.53}Ga_{0.47}As$ HEMTs with extrinsic transconductance of 1052 mS/mm

ZHONG Ying-Hui[1], WANG Xian-Tai[2], SU Yong-Bo[2], CAO Yu-Xiong[2],
ZHANG Yu-Ming[1], LIU Xin-Yu[2], JIN Zhi[2*]
(1. School of Microelectronics, Xidian University, Xi'an 710071, China;
2. Institute of Microelectronics, Chinese Academy of Sciences, Beijing 100029, China)

Abstract: 0.15 μm gate-length InP-based $In_{0.52}Al_{0.48}As/In_{0.53}Ga_{0.47}As$ high electron mobility transistors (HEMTs) were successfully fabricated with gate-width of 2×50 μm and source-drain space of 2 μm. The maximum extrinsic transconductance (g_m^{ext}) of 1 052 mS/mm was obtained under gate-source voltage (V_{GS}) of 0.1 V and drain-source voltage (V_{DS}) of 1.7 V at room temperature. Transmission Line Method (TLM) measurements revealed the contact resistance of 0.032 Ω·mm and the specific contact resistivity of 1.03×10^{-7} Ω·cm^{-2} on linear TLM patterns. Thus, markedly enhanced g_m^{ext} was achieved by the superb Ohmic contact and the short source-drain space for minimizing series source resistance. These devices also demonstrated excellent RF characteristics. The f_T and f_{max} extrapolated using the *S*-parameters measured from 100 MHz to 40 GHz were 151 GHz and 303 GHz, respectively. The HEMTs were promising for millimeter-wave band integrated circuits.

Key words: HEMT; gate-length; gate recess; InP; InAlAs/InGaAs
PACS: 84.40.-x

有效跨导为1052 mS/mm的高性能InP基 $In_{0.52}Al_{0.48}As/In_{0.53}Ga_{0.47}As$ HEMTs

钟英辉[1], 王显泰[2], 苏永波[2], 曹玉雄[2], 张玉明[1], 刘新宇[2], 金 智[2*]
(1. 西安电子科技大学 微电子学院, 陕西 西安 710071;
2. 中国科学院微电子研究所, 北京 100029)

摘要:成功研制了栅长为0.15 μm、栅宽为2×50 μm、源漏间距为2 μm的InP基$In_{0.52}Al_{0.48}As/In_{0.53}Ga_{0.47}As$高电子迁移率器件.室温下,当器件$V_{DS}$为1.7 V、$V_{GS}$为0.1 V时,其有效跨导达到了1 052 mS/mm.传输线方法(TLM)测试显示器件的接触电阻为0.032 Ω·mm,器件欧姆接触电阻率为1.03×10^{-7} Ω·cm^{-2}.正是良好的欧姆接触及其短的源漏间距减小了源电阻,进而使得有效跨导比较大.器件有比较好的射频特性.从100 MHz到40 GHz, S参数外推出来的f_T和f_{max}分别为151 GHz和303 GHz.所报道的HEMT器件非常适合毫米波段集成电路的研制.

关 键 词:高电子迁移率器件;栅长;栅槽;InP;InAlAs/InGaAs
中图分类号:TN385 **文献标识码**:A

Introduction

Millimeter and sub-millimeter wave devices are of great interests for remote atmospheric sensing, next generation automotive collision avoidance radars, broadband satellite communications and low noise de-

Received date: 2012-03-01, **revised date**: 2012-04-26 **收稿日期**:2012-03-01, **修回日期**:2012-04-26
Foundation items: Supported by the National Basic Research Program of China (2010CB327502)

Biography: Zhong Yinghui (1987-), female, Guang'an, Sichuan, Ph. D candidate. Research field is ultra-high speed millimeter-wave devices and circuits. E-mail: zhongyinghui401@163.com.

* **Corresponding author**: E-mail: jinzhi@ime.ac.cn.

tectors. The InP-based high electron mobility transistors (HEMTs) have demonstrated high frequency, low microwave and millimeter wave noise and high gain performance, due to the high electron carrier density, high peak drift velocity and high mobility in the channel. Therefore, the devices are considered to be one of the most promising devices for those applications. Excellent results of InP-based HEMTs have been reported by different groups, e. g. the current gain cutoff frequency (f_T) of 628 GHz, the maximum oscillation frequency (f_{max}) of 331 GHz, the extrinsic maximum transconductance (g_m^{ext}) of 1.62 S/mm for 30 nm InAs pseudomorphic InP HEMTs[1], f_T = 385 GHz, f_{max} > 1 THz for sub 50 nm InP HEMTs[2] and f_T = 644 GHz, f_{max} = 681 GHz, g_m^{ext} = 2.3 S/mm for 30 nm InAs PHEMTs[3].

When the operating frequency of integrated circuits (ICs) approaches millimeter and sub-millimeter wave band, the size of HEMTs in the ICs must be reduced so as to be treated as lumped parameter elements. However, such reduction decreases the current level and output power of the ICs. The solution to these problems is to ensure a large g_m^{ext} as well as a high drain current density. The g_m^{ext} of HEMTs can be enhanced by reducing the distance between gate and two-dimensional electron gas (d_{GC}) or by minimizing the series source resistance (R_S). The thickness of the epitaxial layers can be controlled very precisely by molecular beam epitaxy (MBE) growth. The critical technological step which determines d_{GC} is the gate recess etching process. It is better to remove the InGaAs cap layer and InP etching-stopper layer completely only with the InAlAs Schottky barrier remained. However, the introduction of InP etching stopper layer as a surface passivation layer can improve the kink effect in DC characteristic[4] and enhance the consistency in gate-recess etching process. Therefore, the g_m^{ext} was enhanced by excellent Ohmic contact and short source-drain space for minimizing R_s with InP etching stopper layer preserved in this work.

In this paper, the design, fabrication, and characteristics of 0.15 μm T-gate InP-based $In_{0.52}Al_{0.48}As$/$In_{0.53}Ga_{0.47}As$ HEMTs were described. g_m^{ext} value as high as 1 052 mS/mm at room temperature has been achieved, benefiting from short source-drain space of 2 μm and excellent Ohmic contact of 0.032 Ω·mm for minimizing series source resistance. These devices also demonstrated excellent RF characteristics: f_T of 151 GHz and f_{max} of 303 GHz. The HEMTs were promising for millimeter-wave band integrated circuits.

1 Multilayer structures

Figure 1 shows a schematic cross-section of the InP HEMTs. The epitaxial layer structure was designed and optimized with parameters shown in Table 1 and grown on 3 inch semi-insulating (100) InP substrate by MBE. The layers, from bottom to top, consisted of an InAlAs buffer, an InGaAs channel, a unstrained InAlAs spacer layer, a Si-doped plane (5×10^{12} cm^{-2}), a 12 nm thick unstrained lnAlAs Schottky barrier layer, an InP etching stopper layer, a composite InGaAs cap layer consisting of a Si-doped $In_{0.6}Ga_{0.4}As$ cap layer (3×10^{19} cm^{-3}) and a Si-doped $In_{0.53}Ga_{0.47}As$ transition layer (5×10^{18} cm^{-3}). The high dopant and high indium content cap layer was grown to facilitate the formation of Ohmic contact, and thus increasing the g_m^{ext} and improving the frequency performance. All InAlAs layers were lattice matched with the InP substrate. The two-dimensional electron gas (2DEG) sheet density was 3.266×10^{12} cm^{-2} and the mobility was 8 000 cm^2/(V·s) at room temperature.

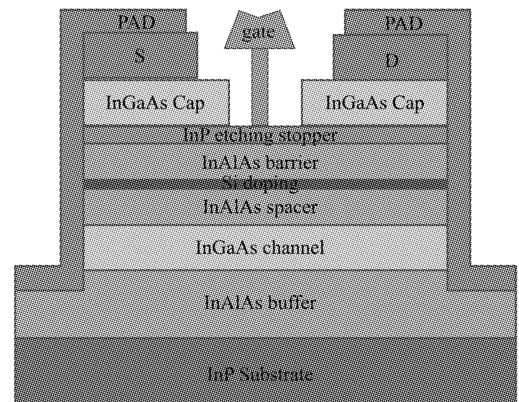

Fig. 1 Schematic cross-section of the InP-based HEMT
图1 InP基HEMT截面图

2 Fabrication process

Figure 2 shows a plane view of the fabricated

Table 1 Device epitaxial layer structure
表 1 器件外延结构

Layer	Material	Doping	Thickness
Cap layer	$In_{0.6}Ga_{0.4}As$	Si:$N^{++}3\times10^{19}(cm^{-3})$	10 nm
Cap layer	$In_{0.53}Ga_{0.47}As$	Si:$N^{+}5\times10^{18}(cm^{-3})$	10 nm
Etch Stop Layer	InP		4 nm
Barrier layer	$In_{0.52}Al_{0.48}As$	Undoped	8 nm
Si planar-doped layer	$5\times10^{12}(cm^{-2})$		
Spacer layer	$In_{0.52}Al_{0.48}As$	Undoped	3 nm
Channel	$In_{0.53}Ga_{0.47}As$	Undoped	15 nm
Buffer layer	$In_{0.52}Al_{0.48}As$	Undoped	500 nm
S. I. InP Sub			

HEMTs with gate width of 2×50 μm and source-drain space (L_{DS}) of 2.0 μm.

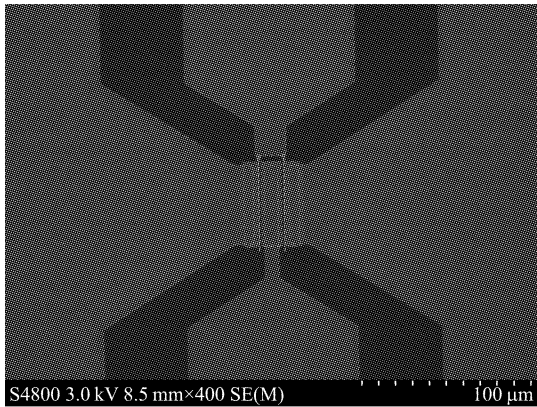

Fig. 2 The SEM photograph of the device
图 2 器件 SEM 照片

The HEMTs' fabrication was based on both optical and electron beam lithography. Firstly, the device isolation was achieved through the mesa formation by means of a phosphorus acid-based wet chemical etching to expose the $In_{0.52}Al_{0.48}As$ buffer layer. Secondly, source and drain Ohmic contact were spaced 2 μm apart by a lift-off process. Then, Ti/Pt/Au was evaporated by an electron beam evaporator to achieve Ohmic metallization without annealing. Transmission Line Method (TLM) measurements revealed the contact resistance of 0.032 Ω · mm and the specific contact resistivity of 1.03×10^{-7} Ω·cm^{-2} on linear TLM patterns. Thirdly, in order to measure on-wafer DC and RF characteristics, the coplanar waveguide bond pads were formed using photoresist AZ5214 and Ti/Au (250/3 000Å) connection wires were evaporated.

The final and most important process in the HEMT fabrication was the gate process, which included gate lithography, recess, and metallization. Firstly, three layers of electron beam (EB) resist of PMMA/Al/UV Ⅲ were coated upon the surface. Then EB exposure and the development of each EB resist layer were carried out in turn. Secondly, the gate recess was formed by a phosphorus acid/hydrogen peroxide wet etching till InP etching-stopper layer, which also served as surface passivation to avoid the kink effect in DC characteristic. Meanwhile, the length of side-etched region (L_{side}) was critical for kink effect, breakdown voltage and frequency performance, and therefore it was optimized to be about 115 nm for the balance. Finally, Ti/Pt/Au gate metal was evaporated and lifted off. The SEM photography of the fabricated 0.15 μm T-gate by EBL and the gate recess details was shown in Fig. 3. During the whole process, no surface passivation was performed. That will cause a parasitic gate-capacitance effect, and then weaken the high-frequency performance.

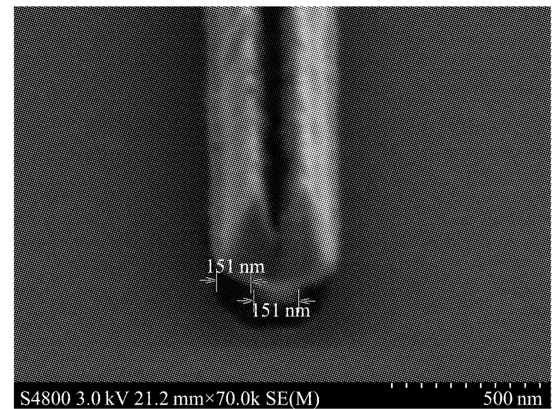

Fig. 3 The SEM photograph of T-gate profile and the gate recess region
图 3 T 型栅及其栅槽腐蚀区域 SEM 照片

3 Results and discussion

The on-wafer DC and RF characteristics of the HEMTs were characterized by a HP4155A semiconductor parameter analyzer and an Agilent E8363B PNA series vector network analyzer at room temperature.

3.1 DC characteristics

Figure 4 shows the current-voltage (I-V) characteristics at room temperature for the HEMTs. The gate-source voltage (V_{GS}) increased from (bottom) -0.3 V to (top) 0.1 V with a step of 0.1 V. It can be seen

from Fig. 4 that the device exhibited no kink effect. Also, good pinch-off characteristics and saturation drain current were observed.

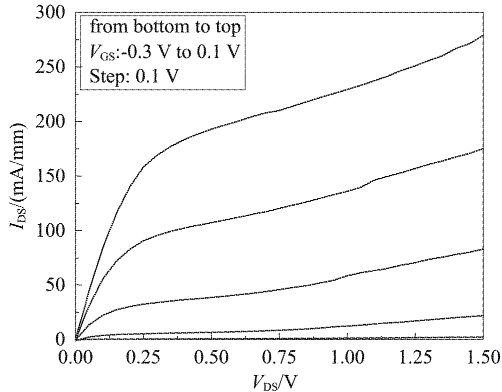

Fig. 4 DC characteristics of the HEMT
图4 HEMT器件的直流特性

Figure 5 demonstrates the gate-bias dependence of extrinsic transconductance and drain current of the HEMT with drain-source voltage (V_{DS}) of 1.7 V. The pinch-off voltage was about -0.4 V. The high dopant and high indium composition pseudomorphic cap layer resulted in a very small non-alloy Ohmic contact with the resistance of 0.032 Ω · mm, and thus benefiting to the extrinsic transconductance. The g_m^{ext} of 1052 mS/mm was obtained at V_{GS} = 0.1 V. The full channel current of 582 mA/mm was measured at V_{GS} of 0.45 V. The gate leakage current was very small (seen from Fig. 6), which was crucial for the lower frequency LNA applications since gate current was a component contributing to shot noise[6].

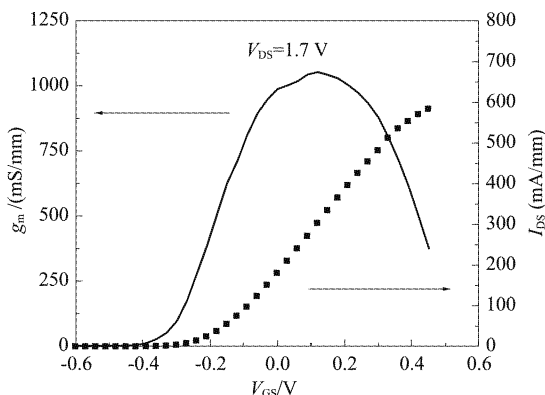

Fig. 5 The dependence of the extrinsic transconductance and drain current on the gate bias of the HEMT
图5 HEMT有效跨导和漏电流随栅偏置的变化关系

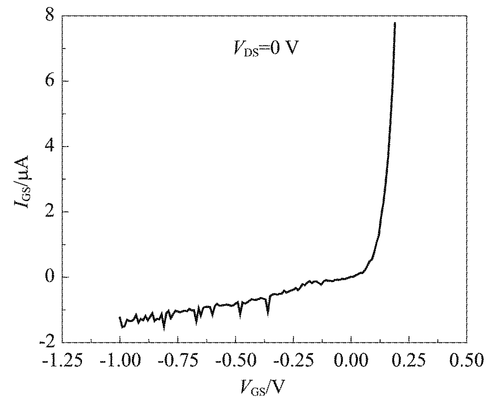

Fig. 6 The gate leakage current of the HEMT
图6 HEMT器件栅漏电

3.2 RF characteristics

The measurements were carried out over the frequency from 0.1 to 40 GHz with step of 0.1 GHz. S-parameter measurements for open and short pads were also performed on the same wafer in order to calibrate the parasitic capacitance and inductance components related to the pad metals. The value of the f_T was determined by extrapolating the current gain (H_{21}) and the f_{max} by extrapolating the maximum available/stable power gain (MAG/MSG) using a least-squares fitting with a -20 dB/decade slope after subtracting the parasitic parameters due to the probing pads.

Figure 7 shows the frequency characteristics of the 0.15 μm gate-length HEMT with V_{DS} of 1.5 V and V_{GS} of 0.1 V after de-embedding the parasitic effects. The extrapolated f_T from H_{21} was 151 GHz and the f_{max} based on MSG/MAG was over 303 GHz. However, it was extrapolated at the instrumentation limit of 40 GHz, where the device was still potentially unstable (K < 1). Extrapolating the gain at -20 dB per decade from this point indicates a larger actual f_{max}. The high RF performance could be attributed to the high extrinsic transconductance of the HEMT. The devices were promising in millimeter-wave band circuits.

3.3 Discussion

Power amplification at high frequencies is very challenging for the device technology development. Both a high output power density (per unit gate periphery) and a large total gate periphery are desirable. However, the size of HEMTs operating in millimeter-wave ICs must be reduced so as to be treated as a lumped param-

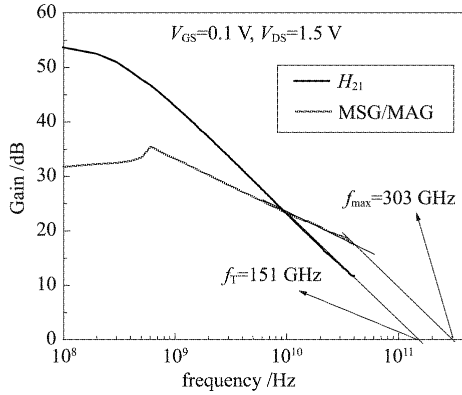

Fig. 7 H_{21} and MAG/MSG versus frequency
图 7 H_{21} 和 MSG/MAG 与频率的关系曲线

eter elements thus decreasing the current level and output power of the ICs. The solution to these problems is to ensure a large g_m^{ext} as well as a high drain current density. The intrinsic and extrinsic transconductance in linear and saturation region can be expressed as:

$$g_{m1}^{int} = \frac{\mu_n W \varepsilon_0 \varepsilon_n}{L d_{GC}} V_{DS} \quad , \quad (1)$$

$$g_{ms}^{int} = \frac{\mu_n W \varepsilon_0 \varepsilon_n}{L d_{GC}} (V_{DS} - V_T) \quad , \quad (2)$$

$$g_{m1}^{ext} = \frac{g_m^{int}}{1 + g_m^{int} R_s + g_d (R_s + R_D)} \quad , \quad (3)$$

$$g_{ms}^{ext} = \frac{g_m^{int}}{1 + g_m^{int} R_s} \quad , \quad (4)$$

where μ_n is the electron mobility, W is the gate-width, ε_0 is the dielectric constant of the air, ε_n is the relatively dielectric constant of the material between the gate and the channel, L is the gate-length.

As seen in the above formulae, the high extrinsic transconductance of the HEMT is mainly related to the high intrinsic transconductance and the low series parasitic resistance, which includes the contact and the access part. Firstly, to achieve high intrinsic transconductance and frequency performance, d_{GC} was controlled precisely by MBE. Secondly, the high dopant and high indium composition pseudomorphic cap layer resulted in very small non-alloy Ohmic contact resistance of 0.032 Ω·mm, and thus benefiting to the extrinsic transconductance. At last, short source-drain space minimized the access part of the series parasitic resistance. The above factors are the main reasons of such high extrinsic transconductance and high frequency performance.

In recent years, InP-based HEMTs have emerged as a promising technology for terahertz applications. Some recorded high frequency characteristics of InGaAs/InAlAs HEMTs, as assessed by f_T and f_{max}, have been published[1-3]. The frequency performance in this paper is lower than these due to the combination of material characteristics and device process. Firstly, the comparatively smaller gate size in these references improves the frequency performance. Secondly, the mobility of the 2DEG reported in Refs. [1-3] is increased by using In-rich channel instead of the lattice matched $In_{0.53}Ga_{0.47}As$ channel in this paper to enhance the breakdown voltage. The lattice-matched channel has the lower mobility of 8 000 $cm^2/(V\cdot s)$. Thirdly, in Ref. [3], the barrier layer thickness of InP based HEMT has been successfully controlled to be 4 nm, which increases the transconductance of the device significantly. However, the barrier layer thickness in our paper is 15 nm, which limits the frequency characteristics in some extent. It's still needed to make further improvement on these issues to enhance the high-frequency performances.

4 Conclusions

0.15 μm gate-length InP-based HEMTs have been fabricated. Due to the epitaxial layer structures designing: the short d_{GC} and high dopant and high indium composition pseudomorphic cap layer, also the short source-drain space, markedly enhanced g_m^{ext} of 1052 mS/mm was achieved. The device also exhibits excellent RF characteristics: f_T and f_{max} of the HEMTs were 151 GHz and 303 GHz respectively. There is room for forward advancement in frequency performance by gate size scaling, an increase of Indium composition in the channel to improve the carrier transport properties, and an improvement of gate recess etching to further decrease the distance from gate to channel. However, the HEMTs are suitable for integrated circuits in millimeter-wave frequencies.

Acknowledgement

The authors appreciate genuinely the help of all

（下转第 288 页）

渐减小且虹特征更加明显,这是因为粒径的增加使得光子被吸收的概率增大而衍射峰越加变窄变高,增大了前向散射.

3 结论

利用颗粒散射理论和辐射传输方程模拟并分析了雪粒的单次散射特征和方向反射率分布函数随粒径大小和入射波长的变化规律,可以得到以下结果.

从积雪的单次散射特性可以看出光子被雪粒反射的概率很高而且具有很强的前向散射,在散射角138°时具有较明显的虹特征;当入射光波长为550nm时,积雪反射率较高且随粒径的变化不明显;而入射光波长为1 640 nm时,由于积雪在该波段的吸收率较高,反射率很低变化同样不明显;入射光波长为1 030 nm时积雪反射率随粒径的变化明显且随观测角度的变化较大,有利于结合光谱和角度信息提高雪粒径的反演精度,同时在利用近红外1 030 nm波段反演雪粒径时还要注意入射天顶角的变化,结合散射角138°时的虹特征进行综合分析可以提高雪粒径的遥感反演精度.

REFERENCES

[1] Aoki T, Aoki T, Fukabori M, *et al.* Effects of snow physical parameters on spectral albedo and bidirectional reflectance of snow surface [J]. *Journal of Geophysical Research*, 2000, **105**(D8): 10219-10236.

[2] Domine F, Albert M, Huthwelker T, *et al.* Snow physics as relevant to snow photochemistry [J]. *Atmospheric Chemistry and Physics*, 2008, **8**(2): 171-208.

[3] Dozier J, Green R O, Nolin A W, *et al.* Interpretation of snow properties from imaging spectrometry [J]. *Remote Sensing of Environment*, 2009, 113: S25-S37.

[4] Wiscombe W J, Warren S G. A Model for the Spectral Albedo of Snow. 1. Pure Snow [J]. *Journal of the Atmospheric Sciences*, 1980, **37**(12): 2712-2733.

[5] Warren S G. Optical properties of snow [J]. *Reviews of Geophysics and Space Physics*, 1982, **20**(1): 67-89.

[6] Colbeck S C. An Overview of Seasonal Snow Metamorphism [J]. *Reviews of Geophysics and Space Physics*, 1982, **20**(1): 45-61.

[7] Dietz A J, Kuenzer C, Gessner U, *et al.* Remote sensing of snow - a review of available methods [J]. *International Journal of Remote Sensing*, 2012, **33**(13): 4094-4134.

[8] Hall D K, Riggs G A, Salomonson V V. Development of methods for mapping global snow cover using moderate resolution imaging spectroradiometer data [J]. *Remote Sensing of Environment*, 1995, **54**(2): 127-140.

[9] Schaepman-Strub G, Schaepman M E, Painter T H, *et al.* Reflectance quantities in optical remote sensing—definitions and case studies [J]. *Remote Sensing of Environment*, 2006, **103**(1): 27-42.

[10] O'Brien H W, Munis R H. Red and near-infrared spectral reflectance of snow [J]. *NASA Goddard Space Flight Center Operational Appl of Satellite Snowcover Observations*, 1975, 345-360.

[11] Li S, Zhou X. Modelling and measuring the spectral bidirectional reflectance factor of snow-covered sea ice: an intercomparison study [J]. *Hydrological Processes*, 2004, 18(18): 3559-3581.

[12] Painter T H, Dozier J. The effect of anisotropic reflectance on imaging spectroscopy of snow properties [J]. *Remote Sensing of Environment*, 2004, **89**(4): 409-422.

[13] Hansen J E, Travis L D. Light scattering in planetary atmospheres [J]. *Space Science Reviews*, 1974, 16: 527-610.

[14] Mishchenko M I, Dlugach J M, Yanovitskij E G, *et al.* Bidirectional refectance of flat, optically thick particulate layers: an efficient radiative transfer solution and applications to snow and soil surfaces [J]. *Journal of Quantitative Spectroscopy & Radiative Transfer*, 1999, 63: 409-432.

[15] Nolin A W, Dozier J. Estimating Snow Grain-Size Using Aviris Data [J]. *Remote Sensing of Environment*, 1993, **44**(2-3): 231-238.

(上接197页)

the members of the IMECAS compound semiconductor device department.

REFERENCES

[1] Lai R, Mei X B, Deal W R, *et al.* Sub 50 nm InP HEMT device with f_{max} greater than 1 THz: IEEE International Electron Devices Meeting IEDM, 2007 [C]. Washington, DC, 2007:609-611.

[2] Kim D-H, del Alamo J A. 30-nm InAs PHEMTs With f_T = 644 GHz and f_{max} = 681 GHz [J]. *IEEE Electron Device Letters*, 2010, **31**(8):806-808.

[3] Kim D-H, del Alamo J A. 30-nm InAs pseudomorphic HEMTs on an InP substrate with a current-gain cutoff frequency of 628 GHz [J]. *IEEE Electron Device Letters*, 2008, **29**(8):830-833.

[4] Zimmer T, Ouro Bodi D, Dumas J M, *et al.* Kink effect in HEMT structures: A trap-related semi-quantitative model and an empirical approach for SPICE simulation [J]. *Solid State Electron*, 1992, **35**(10):1543-1548.

[5] Suemitsu T, Enoki T, Sano N, *et al.* An analysis of the kink phenomena in InAlAs/InGaAs HEMTs using two dimensional device simulation [J]. *IEEE Transactions On Electron Devices*, 1998, **45**(12):2390-2399.

[6] Grundbacher R, Lai R, Barsky M, *et al.* 0.1 μm InP HEMT devices and MMICs for cryogenic low noise amplifiers from X-band to W-band simulation: 14th Indium phosphide and related materials conference IPRM, 2002 [C]. Stockholm, Sweden, 2002:455-458.